Modeling the temperature characteristics of InAs/GaAs quantum dot lasers

Modeling the temperature characteristics of InAs/GaAs quantum dot lasers

Marco Rossetti,[a] Andrea Fiore,[b] Grzegorz Sęk,[c] Carl Zinoni, and Lianhe Li
Ecole Polytechnique Fédérale de Lausanne, CH-1015 Lausanne, Switzerland

(Received 14 March 2009; accepted 16 June 2009; published online 23 July 2009)

A systematic investigation of the temperature characteristics of quantum dot lasers emitting at 1.3 μm is reported. The temperature dependence of carrier lifetime, radiative efficiency, threshold current, differential efficiency, and gain is measured, and compared to the theoretical results based on a rate equation model. The model accurately reproduces all experimental laser characteristics above room temperature. The degradation of laser characteristics with increasing temperature is clearly shown to be associated to the thermal escape of holes from the confined energy levels of the dots toward the wetting layer and the nonradiative recombination therein.
 [DOI: 10.1063/1.3176499]

I. INTRODUCTION

Since their theorization quantum dot (QD) devices have been predicted to show better temperature stability if compared to their quantum well (QW) or bulk counterpart.[1,2] Due to the discrete nature of the QD energy levels, carriers are supposed to experience a smaller thermal dispersion resulting in a lower thermal sensitivity of devices. In spite of these predictions most of the devices realized so far have shown a temperature dependence similar to the one obtained on InP based QWs for 1.3 μm emission, with laser characteristic temperature T_0 smaller than 100 K in the 20–80 °C interval.[3–6] Higher T_0 has been obtained in lasers based on *p*-doped QDs, but at the expense of higher room-temperature (RT) threshold current density.[7–9] To explain the temperature sensitivity of QD lasers, different mechanisms have been proposed in the literature. First, thermal escape of carriers from QDs to the wetting layer (WL) and barriers, and associated *radiative* recombination, has been evoked[8,10–12] to explain the reduced gain and larger threshold current for increasing temperatures. On the other hand, strong evidence for nonradiative (NR) processes—in particular in the WL—has been found in the temperature dependence of both QD photoluminescence (PL)[13,14] and laser characteristics,[15–17] and this process has been incorporated in laser models to reproduce the experimental T_0.[9,16] Indeed, it should be noted that the WL is an In-rich 2D layer which is formed in conditions not optimized for QW growth—a relatively large concentration of NR traps is thus not surprising. Finally, a dominant role of Auger NR recombination at RT has been suggested by the dependence of threshold current as a function of applied pressure[18] and by the nonlinear light-current characteristics.[19] This last explanation is particularly appealing, as Auger processes are known to determine the temperature dependence of InP-based 1.3–1.55 μm QW lasers. Nevertheless, the arguments used to support the role of Auger NR recombination must be carefully analyzed in the specific case of QDs. In fact, the sublinearity of light-current characteristics can be also traced to the easy saturation of QD lower-energy states, and increased evaporation of carriers to WL states, and thus does not prove the existence of Auger-type processes. The decrease in threshold current with pressure is also not a definitive proof of the dominating role of Auger recombination. In fact, as the lasing wavelength decreases with pressure, the mode gets increasingly confined in the waveguide, and the modal gain increases for constant carrier density.[20] The observed 20% decrease in the threshold current for pressures of ≈10 kbar could indeed be due to a ≈10% increase in modal gain associated to the 10% decrease in the lasing wavelength.[18] Additionally, even if Auger recombination contributes a fraction of the threshold current at RT, this process itself does not explain the temperature dependence, unless an *ad hoc* temperature variation in the Auger coefficient is assumed. Indeed, no model has been proposed to interpret the experimental temperature variation in threshold current as due to the increase in Auger recombination (on the contrary, the latter has been suggested to decrease with temperature[8]). In fact, while in bulk or QW active regions the Auger NR recombination scales as $R_A \propto n^3$, leading to a strong temperature dependence if the threshold carrier density n_{th} depends on temperature, this argument does not hold in QDs due to the localized nature of recombination.[21] Indeed, calculated Auger currents cannot explain the experimental T_0,[21] unless an *ad hoc* temperature variation in the Auger cross section is introduced.

In order to discriminate between the different possible mechanisms, the measurement and modeling of several aspects of the material and laser characteristics—not only threshold current—is needed. In this paper, by taking a systematic approach, we gather strong experimental and theoretical evidences supporting the role of thermal escape and monomolecular NR recombination in the WL as the main physical process responsible for the temperature dependence. We focus on the 1.3 μm InAs/GaAs material system. The main contributions with respect to the existing literature are the following: (a) We present direct experimental evidence of

[a]Author to whom correspondence should be addressed. Electronic mail: rossetti@exalos.com. Present address: EXALOS AG, CH-8952 Schlieren, Switzerland.
[b]Present address: COBRA Research Institute, Eindhoven University of Technology, P.O. Box 513, 5600 MB Eindhoven, The Netherlands.
[c]Also at Institute of Physics, Wroclaw University of Technology, 50-370 Wroclaw, Poland.

strong and temperature-dependent *nonradiative* recombination in QDs around RT, from carrier lifetime and radiative efficiency measurements. As the measured values do not show a strong excitation dependence, we attribute this NR recombination to monomolecular processes. (b) We develop a rate equation model (REM) which explicitly treats defect-related NR recombination in the WL by a Shockley–Read–Hall (SRH) approach.[22,23] (c) We show that this model can quantitatively reproduce the temperature dependence, not only of the threshold current, but also of the gain, the laser differential efficiency, and the spontaneous emission (i.e., radiative) efficiency, *using a single, temperature-independent fitting parameter* (NR recombination time in the WL). The temperature dependence is shown in the model to be directly related to hole evaporation to the WL. This set of results strongly supports the role of defect-related NR recombination in the WL in state-of-the-art 1300 nm QD lasers, and suggests that further improvements in material quality could provide substantial benefits to the laser characteristics.

The theoretical model is first presented in Sec. II. The fabricated and investigated QD devices are described in Sec. III. The temperature dependence of the radiative properties and of laser characteristics are discussed in Secs. IV and V, respectively, and conclusions are drawn in Secs. VI and VII.

II. REM

REMs are widely used in literature to model a QD system,[24–28] inspired by the description of average carrier densities in bulk materials, QWs, or quantum wires. In this approach the temporal evolution of carrier populations and photon numbers inside an optical cavity may be modeled through a system of coupled differential equations. For simulation of laser diodes a mean-field model considering all the quantities averaged over the cavity length may be fully satisfactory as the finite reflectivities of the cavity facets make the photon distribution rather uniform across the device length.

Here we report on results obtained with a REM where equations for the electron and hole populations are considered separately—as shown below, this is essential to correctly treat thermal evaporation processes. Four discrete bound states are considered for both conduction and valence bands. In the following we will refer to them as ground state ($GS_{e,h}$), excited state ($ES_{e,h}$), second excited state ($SES_{e,h}$), and third excited state ($TES_{e,h}$), where the indices e or h identify the energy levels in conduction or valence band, respectively. This levels are coupled each other through relaxation and thermal escape mechanisms (inside each band) and through carrier recombination (interband transitions). As far as interband optical transitions are considered, most of the theories predict allowed transitions between states of differing quantum numbers,[29] however the associated oscillator strength is usually lower than for transitions between states of the same quantum numbers. In Ref. 30, for example, dominant transitions between states of the same quantum number have been predicted. The latter prediction was confirmed in a paper of Itskevich *et al.* in 1999,[31] where the spectra of InAs/GaAs self-assembled QDs were analyzed in a condition of varying hydrostatic pressure. The authors identified four principal transitions in the spectra, each one related to the recombination between a different electron and hole level, thus confirming the presence of strict selection rules also for the recombination from the excited energy levels. In analogy, here we consider only optical transitions between energy levels with the same quantum numbers. For this reason, the number of bound states in conduction and valence band is assumed identical and is chosen in agreement with the number of optical transitions observed in these QDs in the high-excitation PL spectra and high-injection electroluminescence spectra. As a term of comparison, calculations for lens-shaped or pyramidal InAs/GaAs QDs similar to the one treated in this paper predict three to five electron states localized in the dots (increasing in general with the sophistication of the model employed), and a similar number of hole states.[29,32] The lower levels show an s symmetry (only spin degeneracy), while the excited states are predicted to have p or even d symmetries (spin and momentum degeneracies). According to theory we have fixed the GS degeneracy to the simple spin degeneracy (2) and increased it for the ES (4), SES (8), and TES (8). The degeneracy ratio between different energy levels was fixed as the ratio of the integrated intensity associated to different transitions in the high-injection electroluminescence spectra measured in the spontaneous emission regime.

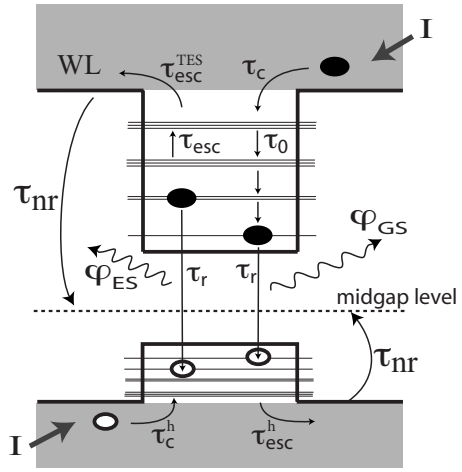

FIG. 1. Schematic of the REM.

The hole levels in the valence band typically show a smaller spacing with respect to the levels in the conduction band,[29] which is mainly due to the larger effective mass of holes. This has been confirmed in a recent work by Sellers *et al.*[33] where the spacing between the electronic ground state transition GS_e and the first excited state ES_e was measured by modulated far-infrared spectroscopy. In analogy with Refs. 29 and 33 we fixed the spacing of energy levels in the valence band as the 20% of the respective interband transition energies (80% for the electrons in the conduction band). The energy for each interband radiative transition was determined through a Gaussian deconvolution of the experimental high-excitation electroluminescence spectra.

A schematic of the energy level structure considered in the REM is shown in Fig. 1, where together with the local-

ized states of the QD, a continuum of states corresponding to the lowest subband of the WL is shown. QDs optimized for emission at 1.3 μm are realized using a 5 nm thick $In_{0.15}Ga_{0.85}As$ capping layer. The system WL capping is electronically coupled and for this reason we have considered it as a single energy level. A NR recombination mechanism through midgap levels is also shown in the picture. This mechanism will be described later in this section. After injection in the GaAs barrier, electron and holes relax to the QD ground state through a complicated dynamics. The first step consists in carrier thermalization within the GaAs barrier and subsequent capture by the WL. This process happens on a timescale of few picoseconds as observed in time-resolved PL experiments by Siegert *et al.*[34] (2 ps), Sun *et al.*[35] (2 ps), and Yuan *et al.*[36] (10 ps) and the carriers, as in the case of a QW, move efficiently across the energy continuum toward the WL band edge. Our model considers a direct injection of carriers into the WL. This assumption is justified by the quick capture of carriers from the separate confinement layers (GaAs) toward the WL, which results in a negligible carrier population in the GaAs even under high electrical injection. In fact, electroluminescence spectra measured from microlight-emitting diodes (LEDs) produced from the same material do not show any evidence of recombination from the GaAs band edge even at current densities much higher then the ones typically used for laser operation. Following barrier to WL capture, the electrons and holes are captured into the less confined state of their respective bands and both proceed toward the GS energy level in a cascade process. Evidence of the cascade process can be found in Refs. 34 and 37, where the rise-time of the time-resolved PL signal was measured at the energies corresponding to different transitions.

The system of ten differential equations describing the populations $n^{e,h}$ of the energy levels in absence of photons can be written as

$$\frac{dn_{\mathrm{WL}}^{e,h}}{dt} = \frac{\mathrm{G}N_D}{\tau_r} + \frac{n_{\mathrm{TES}}^{e,h}}{\tau_{\mathrm{esc}}^{\mathrm{TES}_{e,h}}} - \frac{n_{\mathrm{WL}}^{e,h} f_{\mathrm{WL}}^{h,e}}{\tau_r} - \frac{n_{\mathrm{WL}}^{e,h}(1-f_{\mathrm{TES}}^{e,h})}{\tau_c^{e,h}}, \tag{1}$$

$$\left\{ \frac{dn_{\mathrm{TES}}^{e,h}}{dt} = \frac{n_{\mathrm{WL}}^{e,h}(1-f_{\mathrm{TES}}^{e,h})}{\tau_c^{e,h}} + \frac{n_{\mathrm{SES}}^{e,h}(1-f_{\mathrm{TES}}^{e,h})}{\tau_{\mathrm{esc}}^{\mathrm{SES}_{e,h}}} - \frac{n_{\mathrm{TES}}^{e,h} f_{\mathrm{TES}}^{h,e}}{\tau_r} - \frac{n_{\mathrm{TES}}^{e,h}}{\tau_{\mathrm{esc}}^{\mathrm{TES}_{e,h}}} - \frac{n_{\mathrm{TES}}^{e,h}(1-f_{\mathrm{SES}}^{e,h})}{\tau_0^{e,h}} \right\}, \tag{2}$$

$$\frac{dn_{\mathrm{SES}}^{e,h}}{dt} = \frac{n_{\mathrm{TES}}^{e,h}(1-f_{\mathrm{SES}}^{e,h})}{\tau_0^{e,h}} + \frac{n_{\mathrm{ES}}^{e,h}(1-f_{\mathrm{SES}}^{e,h})}{\tau_{\mathrm{esc}}^{\mathrm{ES}_{e,h}}} - \frac{n_{\mathrm{SES}}^{e,h} f_{\mathrm{SES}}^{h,e}}{\tau_r} - \frac{n_{\mathrm{SES}}^{e,h}(1-f_{\mathrm{TES}}^{e,h})}{\tau_{\mathrm{esc}}^{\mathrm{SES}_{e,h}}} - \frac{n_{\mathrm{SES}}^{e,h}(1-f_{\mathrm{ES}}^{e,h})}{\tau_0^{e,h}}, \tag{3}$$

$$\frac{dn_{\mathrm{ES}}^{e,h}}{dt} = \frac{n_{\mathrm{SES}}^{e,h}(1-f_{\mathrm{ES}}^{e,h})}{\tau_0^{e,h}} + \frac{n_{\mathrm{GS}}^{e,h}(1-f_{\mathrm{ES}}^{e,h})}{\tau_{\mathrm{esc}}^{\mathrm{GS}_{e,h}}} - \frac{n_{\mathrm{ES}}^{e,h} f_{\mathrm{ES}}^{h,e}}{\tau_r} - \frac{n_{\mathrm{ES}}^{e,h}(1-f_{\mathrm{SES}}^{e,h})}{\tau_{\mathrm{esc}}^{\mathrm{ES}_{e,h}}} - \frac{n_{\mathrm{ES}}^{e,h}(1-f_{\mathrm{GS}}^{e,h})}{\tau_0^{e,h}}, \tag{4}$$

$$\frac{dn_{\mathrm{GS}}^{e,h}}{dt} = \frac{n_{\mathrm{ES}}^{e,h}(1-f_{\mathrm{GS}}^{e,h})}{\tau_0^{e,h}} - \frac{n_{\mathrm{GS}}^{e,h} f_{\mathrm{GS}}^{h,e}}{\tau_r} - \frac{n_{\mathrm{GS}}^{e,h}(1-f_{\mathrm{ES}}^{e,h})}{\tau_{\mathrm{esc}}^{\mathrm{GS}_{e,h}}}, \tag{5}$$

where the index e or h differentiates the electron from the hole equations and the intraband carrier transfer from one level toward another is governed by a Pauli-blocking term of the form $(1-f)$ accounting for the occupation f of the arrival level. This term has been expressly neglected in the escape rate from TES to WL because the latter is considered a reservoir with much higher degeneracy. We note also that $f_{\mathrm{WL}}^{e,h}$ is not a proper occupation function but was defined as $f_{\mathrm{WL}}^{e,h} = n_{\mathrm{WL}}^{e,h}/N_D$ in order to maintain charge parity and to properly account for the radiative recombination in the WL. Radiative recombinations are instead expressed as a bimolecular term ($n^e f^h$ or $n^h f^e$), where the probability of electron-hole recombination is proportional to the product of the occupation functions of the energy levels involved in the transition. The lifetime of radiative transitions τ_r is set to 1 ns as measured for the GS transition in low temperature time-resolved PL experiments, and is assumed to be identical also for the transitions from the excited states. The electron capture time τ_c^e from the WL to the TES is fixed to 1 ps, in agreement with Refs. 34 and 35, and the relaxation time τ_0^e between confined energy levels is fixed to 7 ps as determined from the fitting of threshold currents in two-state QD lasers,[26] and is considered identical for all the relaxation mechanisms in conduction band. As capture and relaxation are expected to be much faster in the valence band due to the smaller spacing of the energy levels, the corresponding times are fixed to 1/10 of the electronic values, which falls in the range of values for which a further decrease does not significantly affect the calculations. The carrier dynamics, in fact, is governed by the electronic times for capture and relaxation as soon as the hole times become faster. The current injection is expressed as a function of the number of QDs N_D in the device [first term in the right side of Eq. (1)], of the electron charge e, of the radiative lifetime τ_r and of the adimensional injection coefficient G

$$I = \frac{eGN_D}{\tau_r}, \tag{6}$$

so that G represents the number of eh-pairs injected in the WL per QD and per unit of radiative lifetime τ_r. N_D is then fixed through the dot areal density n_D (set to 3×10^{10} cm^{-2} as determined by atomic force microscopy on uncapped QD samples), the laser size (section parallel to the growth plan), and the number of QD layers in the active region. The thermal escape times τ_{esc}^j from level i may be easily related to τ_c and τ_0 assuming a thermal equilibrium in the absence of external excitation and considering the relative degeneracy of the initial and final state for the transition, which results in the expressions

$$\tau_{\mathrm{esc}}^{\mathrm{TES}_{e,h}} = \tau_c^{e,h} \frac{8N_D \pi \mathbf{h}^2}{m_{\mathrm{eff}}^{e,h} k_B T} \exp\left(\frac{|E_{\mathrm{WL}}^{e,h} - E_{\mathrm{TES}}^{e,h}|}{k_B T} \right), \tag{7}$$

$$\tau_{\mathrm{esc}}^{\mathrm{SES}_{e,h}} = \tau_0^{e,h} \exp\left(\frac{|E_{\mathrm{TES}}^{e,h} - E_{\mathrm{SES}}^{e,h}|}{k_B T} \right), \tag{8}$$

$$\tau_{\mathrm{esc}}^{\mathrm{ES}_{e,h}} = \frac{\tau_0^{e,h}}{2}\exp\left(\frac{|E_{\mathrm{SES}}^{e,h} - E_{\mathrm{ES}}^{e,h}|}{k_B T}\right), \tag{9}$$

$$\tau_{\mathrm{esc}}^{\mathrm{GS}_{e,h}} = \frac{\tau_0^{e,h}}{2}\exp\left(\frac{|E_{\mathrm{ES}}^{e,h} - E_{\mathrm{GS}}^{e,h}|}{k_B T}\right), \tag{10}$$

where the coefficient 2 in Eqs. (9) and (10) accounts for the different degeneracies of GS, ES, and SES. $\tau_{\mathrm{esc}}^{\mathrm{TES}_{e,h}}$ has been derived considering the WL as an $In_{0.15}Ga_{0.85}As$ QW (WL +capping coupled system) and integrating the escape rate over all the energies of the lowest subband. Such assumption is based on the fact that the emission of InAs QDs is extended up to 1.3 μm through the use of a 5 nm thick $In_{0.15}Ga_{0.85}As$ layer capping the dots, which is overlapped to the actual QD WL. The effective mass m_{eff} present in the denominator of Eq. (7) makes the thermal evaporation of carriers from the confined energy levels of the dot toward the WL much faster for the holes than it is for the electrons. This is in our opinion, together with the smaller spacing of the energy levels in valence band, one of the factors having a strong impact on the temperature characteristics of QD lasers.

In the previous equations we considered only radiative interband processes. However, when dealing with the temperature characteristics of QD devices where the NR processes may play an important role, the equations should be updated to account for the effect of NR recombination. One of the main assumptions of the model is that NR recombination only involves free carriers in the WL. In fact, QD carriers are localized and are not affected by NR defects located outside the QD. In contrast, in the 2D WL carrier diffusion allows efficient trapping by defects, which are expected to the large In content and growth conditions which are optimized for the QDs and not necessarily for the WL. The NR recombination is introduced in the model in the form of a SRH term added to the electron [Eq. (1)]

$$-\frac{n_{\mathrm{WL}}^{e}(1 - f_{\mathrm{mg}})}{\tau_{\mathrm{NR}}}, \tag{11}$$

and to the hole [Eq. (1)]

$$-\frac{n_{\mathrm{WL}}^{h} f_{\mathrm{mg}}}{\tau_{\mathrm{NR}}}. \tag{12}$$

The two terms describe the independent capture of electrons and holes from the WL into midgap defects. τ_{NR} is the capture time in the trap states (assumed to be the same for electrons and holes) and $f_{\mathrm{mg}} = n_{\mathrm{mg}}/D_{\mathrm{mg}}$, where n_{mg} is the population of electrons trapped in the defects and D_{mg} is the number of defects, which we assume equal to the number of dots. Such assumption is justified by the fact that the presence of defects in the combined QD+capping structure can be attributed to strain relaxation induced by the QD nucleation. The actual defect density is however difficult to access experimentally due to the high degree of complexity of the full laser structure and the value assumed here is only a first approximation. We then add one more equation to the rate equation system to describe the temporal evolution of n_{mg}

$$\frac{dn_{\mathrm{mg}}}{dt} = \frac{n_{\mathrm{WL}}^{e}(1 - f_{\mathrm{mg}}) - n_{\mathrm{WL}}^{h} f_{\mathrm{mg}}}{\tau_{\mathrm{NR}}}, \tag{13}$$

where the electron-hole recombination is assumed instantaneous and the thermal escape from the midgap level is neglected due to the large energy spacing from the WL. As will be shown in the following paragraphs the lifetime τ_{NR} has a strong impact on the temperature characteristics of the laser and will be used as a fitting parameter to reproduce threshold currents and slope efficiency variations in real lasers. We note that explicitly including the defect level in the model allows the treatment of NR recombination while conserving the total charge in the system, differently from the approach[38] where a $dn_{\mathrm{WL}}^{e,h}/dt|_{\mathrm{NR}} = -n_{\mathrm{WL}}^{e,h}/\tau_{\mathrm{NR}}$ term is directly included in the QD population Eqs. (1)–(5).

To account for the presence of photons, the contributions of absorption and stimulated emission must be added to Eqs. (2)–(5). The temporal evolution of the average photon number in the guided mode φ_{TES}, φ_{SES}, φ_{ES}, and φ_{GS} associated to each radiative transition is described through a further set of rate equations governed by spontaneous emission, stimulated emission, and photon losses. For the case of a laser operating on the GS transition, the third and second excited states (TES and SES) are far from reaching positive optical gain and the corresponding photon equations and gain terms to be added to Eqs. (2) and (3) can generally be neglected. For completeness here we consider all the equations

$$\frac{d\varphi_{\mathrm{TES}}}{dt} = \beta\frac{n_{\mathrm{TES}}^{e} f_{\mathrm{TES}}^{h}}{\tau_r} - \frac{\varphi_{\mathrm{TES}}}{\tau_\varphi} + \varphi_{\mathrm{TES}} B_{\mathrm{TES}}(n_{\mathrm{TES}}^{e} + n_{\mathrm{TES}}^{h} - 8N_D), \tag{14}$$

$$\frac{d\varphi_{\mathrm{SES}}}{dt} = \beta\frac{n_{\mathrm{SES}}^{e} f_{\mathrm{SES}}^{h}}{\tau_r} - \frac{\varphi_{\mathrm{SES}}}{\tau_\varphi} + \varphi_{\mathrm{SES}} B_{\mathrm{SES}}(n_{\mathrm{SES}}^{e} + n_{\mathrm{SES}}^{h} - 8N_D), \tag{15}$$

$$\frac{d\varphi_{\mathrm{ES}}}{dt} = \beta\frac{n_{\mathrm{ES}}^{e} f_{\mathrm{ES}}^{h}}{\tau_r} - \frac{\varphi_{\mathrm{ES}}}{\tau_\varphi} + \varphi_{\mathrm{ES}} B_{\mathrm{ES}}(n_{\mathrm{ES}}^{e} + n_{\mathrm{ES}}^{h} - 4N_D), \tag{16}$$

$$\frac{d\varphi_{\mathrm{GS}}}{dt} = \beta\frac{n_{\mathrm{GS}}^{e} f_{\mathrm{GS}}^{h}}{\tau_r} - \frac{\varphi_{\mathrm{GS}}}{\tau_\varphi} + \varphi_{\mathrm{GS}} B_{\mathrm{GS}}(n_{\mathrm{GS}}^{e} + n_{\mathrm{GS}}^{h} - 2N_D), \tag{17}$$

where B_{GS}, B_{ES}, B_{SES}, and B_{TES} are the Einstein coefficients for absorption and stimulated emission. The coefficient β is the spontaneous emission coupling factor accounting for the fraction of spontaneously emitted photons that are coupled in the guided mode. This is of the order of 10^{-5} for a laser diode.[39] The photon lifetime τ_φ is related to the photon losses due to the finite reflectivity of the cavity facets (mirror loss α_m) and due to the photon scattering at the etched waveguide sidewalls or to free-carrier absorption (internal loss α_i)

$$\tau_\varphi = \frac{n_{\mathrm{eff}}}{c(\alpha_m + \alpha_i)}, \tag{18}$$

where n_{eff} is the effective index for the guided mode.

Equations (2)–(5) must then be corrected introducing the term accounting for absorption and stimulated emission

$$- \varphi_{TES} B_{TES} (n^e_{TES} + n^h_{TES} - 8N_D), \quad (19)$$

$$- \varphi_{SES} B_{SES} (n^e_{SES} + n^h_{SES} - 8N_D), \quad (20)$$

$$- \varphi_{ES} B_{ES} (n^e_{ES} + n^h_{ES} - 4N_D), \quad (21)$$

$$- \varphi_{GS} B_{GS} (n^e_{GS} + n^h_{GS} - 2N_D). \quad (22)$$

The rate equations presented can be used to model the *LI* curves of QD lasers and can also be applied to reproduce their temperature characteristics. In the next sections we compare the experimental results obtained on lasers containing ten QD layers with the REM calculations.

III. DEVICE FABRICATION

The lasers presented in this paper were realized from a *p-i-n* epitaxial structure grown by molecular beam epitaxy consisting in 1.5 μm thick $Al_{0.35}Ga_{0.65}As$ claddings doped *p* (top) and *n* (bottom) and a 450 nm thick intrinsic GaAs core region containing ten QD layers. The (undoped) QDs were obtained in the Stranski–Krastanow mode by continuous deposition of a InAs layer, and capped by an InGaAs layer to shift the GS emission peak toward the 1300 nm range. The layers were largely spaced to avoid possible coupling effects and to reduce the impact of strain on the quality of the active material. Lasers were then realized by dry etching 3 μm wide ridge waveguides, passivating the etched region with benzocyclobutene and depositing *p*- and *n*-contacts by electron-beam evaporation. Laser facets were finally created by cleaving. These devices operate at RT with a lasing peak at 1275 nm and a threshold current density of 180 A/cm^2 for 2 mm long cavities with as-cleaved facets. Besides lasers, the same process was also used to fabricate tilted waveguides (7° tilted to the output facets). These devices operate as single pass amplifiers and the absence of optical feedback allows the evaluation of modal gain in the QD active region.

IV. TEMPERATURE DEPENDENCE OF THE RADIATIVE PROPERTIES

We first present the temperature-dependent radiative properties of these QDs. To experimentally check the hypothesis of increased non-radiative recombination for increasing temperature, the PL decay time for the GS transition was measured by time-resolved PL as a function of temperature on test samples (undoped, no waveguide) containing QDs grown under analogous conditions to the one used for the laser growth. The PL decay time was measured by exciting the sample with a pulsed diode laser (λ=750 nm, pulse width=50 ps) in a micro-PL setup, filtering the PL from the GS with a high-pass filter, coupling the PL to a single-photon detector (InGaAs avalanche photodiode) and building histograms of the laser-PL delay with a correlation card. The temporal decays measured at a fixed excitation density of ~1 W/cm^2 (low enough that the GS is far from saturation), are shown in Fig. 2(a) for different sample temperatures from 10 to 323 K. As the set-up temporal resolution is limited to 600 ps by the detector jitter, the measured decays were fitted with a monoexponential convoluted with

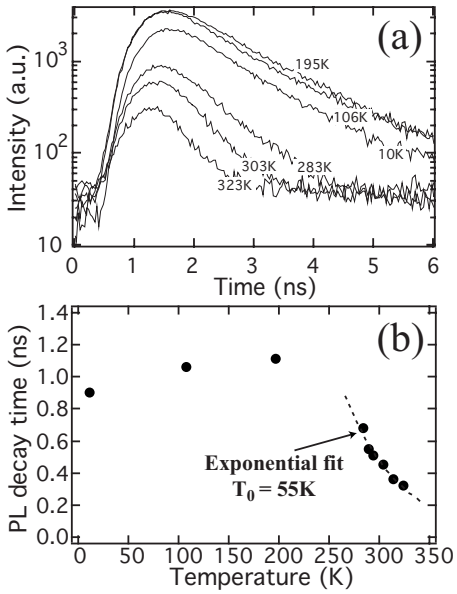

FIG. 2. (a) PL temporal decays measured at the GS transition on a reference QD sample for varying temperature. (b) Corresponding decay times. The dashed line is an exponential fit.

the measured set-up response to derive the PL decay time. The resulting lifetimes are shown in Fig. 2(b). The dotted line is an exponential fit in the high-temperature regime. At low temperature (10–200 K) the measured lifetime is expected to be mainly related to radiative recombinations as the PL intensity does not suffer from thermal degradation. The slight increase in lifetime can therefore be related to an increase in thermal spreading of holes over the valence band energy levels and the consequent increase in the radiative lifetime τ_r (decreased probability of radiative recombination), as previously observed in these 1300 nm QDs.[40] The behavior is reversed around and above RT, where the decay time undergoes a rapid decrease. We note that the lifetime dependence *above* RT was never addressed before to the best of our knowledge. This decrease corresponds to the well-known decrease in the integrated PL intensity, which therefore must be related to increased NR recombinations. A decreasing exponential fit of the decay times in the high-temperature regime results in a characteristic temperature T_0 of 55 K. As discussed in the next paragraph, this is similar to the characteristic temperature of lasers and suggests that the increasing rate of NR recombination is also at the origin of the threshold current increase in lasers. We note that in the literature the characteristic temperature T_0 is usually associated to the temperature increase in threshold currents in a semiconductor laser. Here we intentionally extend the concept of characteristic temperature to the decay times of the PL (and in the next paragraph to the external efficiency of short tilted ridge-waveguide devices) to stress the fact that the temperature behavior of all these quantities is governed by the same microscopic mechanism.

To further quantify this NR mechanism, we have measured the external electroluminescence efficiencies measured ex-facet from short tilted ridge-waveguide devices (L =500 μm) at low injection, where gain and losses are negligible. In such a device (operating as a LED) the effects

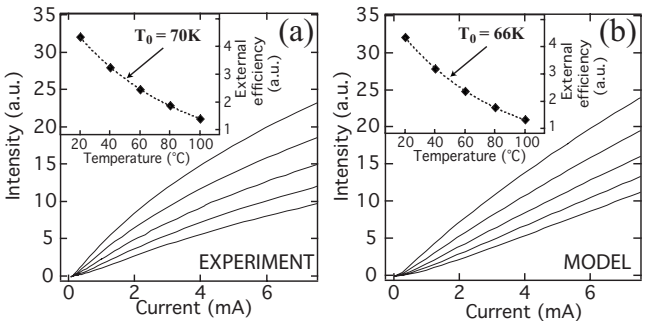

FIG. 3. Measured (a) and calculated (b) *LI* characteristics of short tilted ridge-waveguide devices (500 μm). In inset: corresponding external quantum efficiencies vs temperature in the low injection regime (gain negligible). The dashed lines are exponential fits.

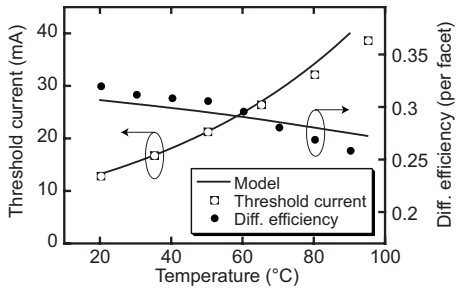

FIG. 4. Threshold currents and differential efficiencies (per facet) vs temperature of a 2 mm long and 3 μm wide ridge-waveguide laser containing 10 QD layers. Experimental data (symbols) and calculations performed with the REM (continuous lines).

related to stimulated emission and absorption can be neglected resulting in a simple dependence on the radiative efficiency (ratio of generated photons to injected electrons, depending on radiative and NR lifetimes). Figure 3(a) shows the measured light-current characteristics for temperatures ranging from 20 to 100 °C. As the extraction efficiency is not expected to vary with temperature, the observed temperature variations can be ascribed solely to varying radiative efficiency. The curves are approximately linear at low currents (<1 mA, corresponding to 50 A/cm^2), with a slope depending on temperature [dots in the inset of Fig. 3(a)]. The low injection differential efficiency in inset was also fitted with a monoexponential, resulting in a characteristic temperature T_0=70 K, close to the value obtained for the PL decays. Qualitatively, this is not the type of nonlinear dependence expected from Auger-dominated recombination (we note that in QDs the usual dependence of Auger recombination $R_A \propto n^3$ does not necessarily hold,[21] and a quantitative analysis of these *LI* characteristics would require specific assumptions about the Auger process). In contrast, we can easily fit these curves using our model [calculated *LI* are displayed in Fig. 3(b)]: A good agreement between model and experiment is obtained simply adjusting the lifetime of capture from the WL to the midgap defects to the temperature-independent value τ_{NR}=10 ps. We stress that this was the only fitting parameter (fixed in all simulations presented throughout the paper) used to reproduce the experimental characteristics and that all the remaining model time constants were determined as described in the previous section. Even though the NR lifetime is surprisingly short, it is not surprising if the WL contains a large number of structural imperfections because it results from the decomposition of the InAs layer consumed by the nucleation process. Such NR lifetime is unfortunately not directly accessible by time-resolved PL experiments.

The calculated external efficiencies versus T are shown in the inset of Fig. 3(b), where they were scaled to the measured value by a constant factor to account for the unknown extraction efficiency. The exponential fit for the calculated extraction efficiencies results in T_0=66 K and a very good agreement between model and experiment is obtained.

These results qualitatively and quantitatively indicate that a single, monomolecular, NR channel is responsible for the observed temperature characteristics of QDs around RT. Indeed, at high temperatures and due to the inhomogeneous character of the WL, the short (10 ps) WL lifetime can only be associated to NR recombination (and indeed no WL emission is observed at these injection levels). If carrier evaporation to the WL and ≈nanosecond-range radiative recombination in the WL, was responsible for the temperature dependence of the threshold current, as suggested in Refs. 8 and 10–12, an increase in carrier lifetime at constant carrier injection would be observed, contrary to the experimental observation. While the expected temperature dependence of lifetime and radiative efficiency in the case of Auger-dominated recombination depends on the details of the Auger process, we expect that a strong dependence on injection level would be seen, and that at sufficiently low injections the radiative efficiency would become temperature-independent. This is in contrast with the experiments described above and with the widely observed decrease in PL efficiency above RT, at all injection levels.

V. TEMPERATURE-DEPENDENT LASER CHARACTERISTICS

We now analyze the temperature dependence of laser and gain characteristics, and compare it to the model. Figure 4 shows the measured threshold current (empty symbols) and differential efficiency (filled symbols) versus temperature of a 2 mm long and 3 μm wide ridge-waveguide laser with as-cleaved facets. The threshold current I_{th} follows an exponential increase with a characteristic temperature of about 70 K. This value of T_0 is typical of low-threshold 1.3 μm lasers with undoped QDs (see, e.g., Refs. 9, 15, 19, and 41). The increase in I_{th} is associated to a decrease in external differential efficiency per facet, which varies from 0.32 at 20 °C to 0.26 at 90 °C. The graph also displays the curves for threshold and efficiency calculated from the steady-state solutions of the REM (continuous lines). The same WL NR lifetime τ_{NR}=10 ps, as fitted from the radiative efficiency measurements above, is used in these calculations. The agreement is very good both for the threshold current and for the efficiency. The phenomenon driving the increase in threshold current and corresponding decrease in differential efficiency is indeed the thermal escape of holes toward the

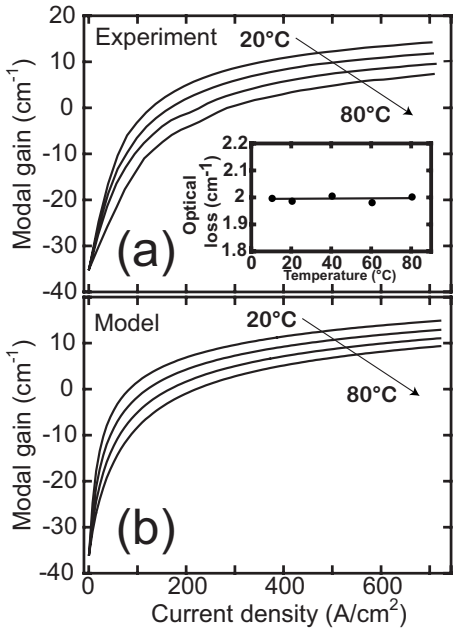

FIG. 5. (a) Net modal gain curves (TE polarization) for varying operating temperature measured on 2 mm long tilted ridge-waveguide amplifiers fabricated from the same wafer used for the lasers. A temperature-dependent measurement of optical internal loss is displayed in inset. (b) Corresponding gain curves calculated with the REM.

WL continuum of states. In order to maintain the threshold carrier population on the GS, an increasing number of carriers must be injected with increasing temperature, which are consumed by NR recombination in the WL.

A better understanding of the device temperature characteristics can be achieved through the analysis of the modal gain and internal loss for varying temperature. First, the internal loss was obtained at RT measuring the fringe visibility of the Fabry–Perot transmission pattern measured injecting a tunable laser (tuned out of resonance) in the laser cavity. Then, its temperature variation was estimated measuring the transmitted intensity of the tunable laser (at a fixed wavelength) through a 2 mm long tilted waveguide for varying operating temperature. The resulting values are shown as a function of temperature in the inset of Fig. 5(a). Similar values were obtained from the fit of the differential external efficiency on lasers with different cavity lengths. A temperature-independent value of 2 cm^{-1} is obtained, confirming that the laser temperature performance is not affected by optical loss. In contrast, the exponential increase in threshold current is fully explained by the degradation of the gain characteristics whose saturation becomes faster for increasing temperature. The modal gain was obtained measuring the amplification of a tunable laser injected into a 2 mm long tilted waveguide realized from the same wafer. The tilting ensures a suppression of the optical feedback and results in a single pass amplification for the injected laser, whose output value can therefore be directly related to the modal gain in the device. Injection and collection of the tunable laser tuned at the GS peak transition was achieved using single-mode, antireflection-coated, lensed fibers. The net modal gain curves for TE polarization (electric field parallel to the growth plan) are displayed in Fig. 5(a) versus current density for the operating temperature of 20, 40, 60, and 80 °C. The curves show a gain decrease versus temperature that is at the origin of the increasing threshold currents in lasers. The measured values are consistent with the measured threshold currents reported in Fig. 1 assuming an internal loss of 2 cm^{-1}, thus confirming that the gain temperature variation—through the NR mechanism described above—is at the origin of the laser T_0. Figure 5(b) shows the modal gain curves calculated with the REM at the steady state. The model accurately reproduces the experimental gain curves without requiring any fitting parameter (same parameters used for the threshold current calculations). We note that even at 20 °C the modal gain curves saturate at a value below 20 cm^{-1}, which is considerably lower than the maximum absorption (40 cm^{-1}) extrapolated at zero injection. This is due to the close spacing of the energy levels in the valence band and the consequent accumulation of holes on the excited energy levels and on the WL where the large degeneracy favors the process of thermal escape. Similarly, the increased thermal escape of holes and consequent NR recombination is also at the origin of the degradation of the gain curves with increasing temperature.

VI. DISCUSSION

Our results show how the temperature dependence of radiative efficiency, gain, threshold current, and differential efficiency in undoped QD lasers can be explained through the simple process of thermal escape toward the WL (particularly strong for the holes due to the vicinity of the energy levels and high degeneracy of the WL) and consequent NR recombination. The experimental results provide a strong additional support to previous investigations on the same mechanisms,[9,16,17,42] which were limited to the analysis of threshold current, and are fully understood by a model which for the first time explicitly treats defect-assisted NR recombination. The devices investigated have the typical characteristics of low-threshold and high-modal gain lasers based on 1.3 μm undoped QDs, so we expect that the same NR process dominates the temperature dependence of most lasers demonstrated so far. Nevertheless, the NR lifetime in the WL strongly depends on the crystal quality and thus on growth conditions. It is therefore in principle possible to produce lasers where NR recombination in the WL is much lower and the Auger process becomes dominant. Indeed, lasers with the lowest demonstrated threshold current densities[43–45] may already be operating in this regime. Additionally, we have restricted our investigation to lasers using undoped QDs in the active region. Lasers with *p*-doped QDs show different and intriguing features, such as very high or even negative T_0 below and around RT (see, e.g., Refs. 7–9), which cannot be understood in the framework of the model presented here due to the absence of Auger-like recombinations and to the fact that we have neglected the spectral dispersion. Indeed, we expect that Auger processes will play a more important role in *p*-doped QDs due to the larger number of carriers, and add an additional NR loss with a different temperature dependence, as proposed in Ref. 8. Another possible force driving the T_0 of *p*-doped lasers toward negative values is the

carrier redistribution inside the gain spectrum due to thermalization, which tends to happen at higher temperatures if compared to undoped QDs due to coulomb interactions.[17] A photon-coupling mechanism has also been proposed[9] to explain the negative T_0. Nevertheless, we note that in all doped QD lasers a strong temperature dependence—similar to the one described here for undoped QDs—is observed at temperatures above RT. The NR loss channel due to thermal escape and NR recombination in the WL thus seems to represent the real limitation to high-temperature performance even for *p*-doped QDs.

VII. CONCLUSIONS

In this article we report a detailed analysis of the temperature characteristics of lasers based on undoped In(Ga)As QDs emitting around 1300 nm. The temperature dependence of carrier lifetime, radiative efficiency, threshold current, differential efficiency, and gain is reported, and compared to the theoretical results based on a REM. In the model, the monomolecular NR recombination in the WL is considered explicitly by introducing a defect level and treating electrons and holes separately. The comparison between model and experiment suggests that the main mechanism behind thermal degradation of laser characteristics around RT is the escape of carriers toward the WL and the following NR recombination. The dominating carrier loss process is the escape of holes due to the smaller spacing of the energy levels in the valence band and to the large density of states of the WL corresponding to the large effective mass. Introducing a fast capture (10 ps) of carriers from the WL toward midgap defects the model accurately reproduces the increase in threshold current and decrease in differential efficiency of lasers, the modal gain curves for varying temperature and the radiative efficiency of LEDs.

ACKNOWLEDGMENTS

The authors are grateful to A. Kovsh, I. Krestnikov, and S. Mikhrin (Innolume GmbH) for growing the samples used in this study, and to P. Voisin (CNRS-LPN) for useful discussions. The authors acknowledge financial support from the EU FP6 integrated project "ZODIAC," Contract No. 17140, the CTI-TOPNANO21 program, Contract No. 6389.1, and the Swiss National Science Foundation.

[1]Y. Arakawa and H. Sakaki, Appl. Phys. Lett. **40**, 939 (1982).
[2]R. Dingle and C. H. Henry, U.S. Patent No. 3982207 (September 21, 1976).
[3]G. T. Liu, A. Stintz, H. Li, T. C. Newell, A. L. Gray, P. M. Varangis, K. J. Malloy, and L. F. Lester, IEEE J. Quantum Electron. **36**, 1272 (2000).
[4]G. Park, O. B. Shchekin, D. L. Huffaker, and D. G. Deppe, Electron. Lett. **36**, 1283 (2000).
[5]A. R. Kovsh, N. A. Maleev, A. E. Zhukov, S. S. Mikhrin, A. P. Vasilev, Yu. M. Shernyakov, M. V. Maximov, D. A. Livshits, V. M. Ustinov, Zh. I. Alferov, N. N. Ledentsov, and D. Bimberg, Electron. Lett. **38**, 1104 (2002).
[6]R. Krebs, F. Klopf, J. P. Reithmaier, and A. Forchel, Jpn. J. Appl. Phys., Part 1 **41**, 1158 (2002).
[7]O. B. Shchekin, J. Ahn, and D. G. Deppe, Electron. Lett. **38**, 712 (2002).
[8]S. Fathpour, Z. Mi, P. Bhattacharya, A. R. Kovsh, S. S. Mikhrin, I. L. Krestnikov, A. V. Kozhukhov, and N. N. Ledentsov, Appl. Phys. Lett. **85**, 5164 (2004).
[9]C. Y. Jin, T. J. Badcock, H.-Y. Liu, K. M. Groom, R. J. Royce, D. J. Mowbray, and M. Hopkinson, IEEE J. Quantum Electron. **42**, 1259 (2006).
[10]L. V. Asryan and R. A. Suris, IEEE J. Quantum Electron. **34**, 841 (1998).
[11]H. Huang and D. G. Deppe, IEEE J. Quantum Electron. **37**, 691 (2001).
[12]C. Z. Tong, S. F. Yoon, C. Y. Ngo, C. Y. Liu, and W. K. Loke, IEEE J. Quantum Electron. **42**, 1175 (2006).
[13]G. Bacher, C. Hartmann, H. Schweizer, T. Held, G. Mahler, and H. Nickel, Phys. Rev. B **47**, 9545 (1993).
[14]R. Heitz, I. Mukhametzhanov, A. Madhukar, A. Hoffmann, and D. Bimberg, J. Electron. Mater. **28**, 520 (1999).
[15]M. Sugawara, K. Mukai, and Y. Nakata, Appl. Phys. Lett. **75**, 656 (1999).
[16]M. Grundmann, O. Stier, S. Bognar, C. Ribbat, F. Heinrichsdorff, and D. Bimberg, Phys. Status Solidi A **178**, 255 (2000).
[17]I. C. Sandall, P. M. Smowton, J. D. Thomson, T. Badcock, D. J. Mowbray, H. Y. Liu, and M. Hopkinson, Appl. Phys. Lett. **89**, 151118 (2006).
[18]I. P. Marko, A. D. Andreev, A. R. Adams, R. Krebs, J. P. Reithmaier, and A. Forchel, IEEE J. Sel. Top. Quantum Electron. **9**, 1300 (2003).
[19]I. P. Marko, A. R. Adams, S. J. Sweeney, D. J. Mowbray, M. S. Skolnick, H. Y. Liu, and K. M. Groom, IEEE J. Sel. Top. Quantum Electron. **11**, 1041 (2005).
[20]P. Adamiec, R. Bohdan, A. Bercha, F. Dybala, W. Trzeciakowski, Y. Rouillard, and A. Joullié, Phys. Status Solidi B **244**, 187 (2007).
[21]P. Blood, H. Pask, H. D. Summers, and I. Sandall, IEEE J. Quantum Electron. **43**, 1140 (2007).
[22]W. Shockley and W. T. Read, Phys. Rev. **87**, 835 (1952).
[23]R. N. Hall, Phys. Rev. **87**, 387 (1952).
[24]M. Sugawara, K. Mukai, and H. Shoji, Appl. Phys. Lett. **71**, 2791 (1997).
[25]S. Sanguinetti, M. Henini, M. Grassi Alessi, M. Capizzi, P. Frigeri, and S. Franchi, Phys. Rev. B **60**, 8276 (1999).
[26]A. Markus, J. X. Chen, O. Gauthier-Lafaye, J. G. Provost, C. Paranthoen, and A. Fiore, IEEE J. Sel. Top. Quantum Electron. **9**, 1308 (2003).
[27]A. A. Dikshit and J. M. Pikal, IEEE J. Quantum Electron. **40**, 105 (2004).
[28]P. Dawson, O. Rubel, S. D. Baranovskii, K. Pierz, P. Thomas, and E. O. Göbel, Phys. Rev. B **72**, 235301 (2005).
[29]A. J. Williamson, L. W. Wang, and A. Zunger, Phys. Rev. B **62**, 12963, (2000).
[30]M. A. Cusack, P. R. Briddon, and M. Jaros, Phys. Rev. B **56**, 4047 (1997).
[31]I. E. Itskevich, M. S. Skolnick, and D. J. Mowbray, Phys. Rev. B **60**, R2185 (1999).
[32]L. W. Wang, A. J. Williamson, A. Zunger, H. Jiang, and J. Singh, Appl. Phys. Lett. **76**, 339 (2000).
[33]I. R. Sellers, D. J. Mowbray, T. J. Badcock, J. P. R. Wells, P. J. Phillips, D. A. Carder, H. Y. Liu, K. M. Groom, and M. Hopkinson, Appl. Phys. Lett. **88**, 081108 (2006).
[34]J. Siegert, S. Marcinkevicius, and Q. X. Zhao, Phys. Rev. B **72**, 085316 (2005).
[35]K. W. Sun, J. W. Chen, B. C. Lee, C. P. Lee, and A. M. Kechiantz, Nanotechnology **16**, 1530 (2005).
[36]Z. L. Yuan, E. R. A. D. Foo, J. F. Ryan, D. J. Mowbray, M. S. Skolnick, and M. Hopkinson, Physica B **272**, 12 (1999).
[37]T. Müller, W. Parz, F. F. Schrey, G. Strasser, and K. Unterrainer, Semicond. Sci. Technol. **19**, S287 (2004).
[38]E. A. Viktorov, P. Mandel, Y. Tanguy, J. Houlihan, and G. Huyet, Appl. Phys. Lett. **87**, 053113 (2005).
[39]Y. Zhao, W. Han, J. Song, X. Li, Y. Liu, D. Gao, G. Du, H. Cao, and R. P. H. Chang, J. Appl. Phys. **85**, 3945 (1999).
[40]A. Fiore, P. Borri, W. Langbein, J. M. Hvam, U. Oesterle, R. Houdré, R. P. Stanley, and M. Ilegems, Appl. Phys. Lett. **76**, 3430 (2000).
[41]X. Huang, A. Stintz, C. P. Hains, G. T. Liu, J. Cheng, and K. J. Malloy, Electron. Lett. **36**, 41 (2000).
[42]Y. Qiu, P. Gogna, S. Forouhar, A. Stintz, and L. F. Lester, Appl. Phys. Lett. **79**, 3570 (2001).
[43]G. Liu, A. Stintz, H. Li, K. J. Malloy, and L. F. Lester, Electron. Lett. **35**, 1163 (1999).
[44]G. Park, O. B. Shchekin, D. L. Huffaker, and D. G. Deppe, IEEE Photon. Technol. Lett. **12**, 230 (2000).
[45]I. R. Sellers, H. Y. Liu, K. M. Groom, D. T. Childs, D. Robbins, T. J. Badcock, M. Hopkinson, D. J. Mowbray, and M. S. Skolnick, Electron. Lett. **40**, 1412 (2004).